

LAND COVER CLASSIFICATION USING E-SAR POLARIMETRIC DATA

V. Karathanassi*, M. Dabboor

Laboratory of Remote Sensing, School of Rural and Surveying Engineering, National Technical University of Athens,
Heron Polytechniou 9, Zographos, 15780, Greece
(karathan*,md2003)@(survey).ntua.gr

Commission VII, WG VII/3

KEY WORDS: Land cover, Polarization, Detection, SAR, Accuracy, Theory, Test

ABSTRACT:

Different decomposition approaches have been proposed in order to analyse and interpret SAR polarimetric images. These are based either on the complex voltage reflection matrix, like Pauli, or on power reflection matrix, like the covariance or coherency matrix. They produce polarimetric parameters which are appropriate to retrieve information on the scattering process of the target. If the target is distributed, polarimetric parameters are affected by speckle.

The objectives of this work are to search and point out the parameters most appropriate for the interpretation of different land uses in a ESAR image; to evaluate Maximum Likelihood (ML) classification results produced by two different polarimetric input sets: the full polarimetric, and the Pauli images; to investigate the most appropriate size of the Lee filter window for polarimetric speckle reduction.

Based on the full polarimetric L-band, polarization signatures were extracted and analyzed for four land cover classes: urban, forest, vegetation and smooth surfaces. The scattering mechanism of these land cover classes was also analysed based on the images generated by Pauli decomposition analysis. The Maximum Likelihood classification was performed on the “magnitude content” of the a) original polarimetric data, b) images produced by the Pauli analysis, and c) both previous cases data. The accuracy of each class confirmed the contribution of polarimetric data and Pauli parameters in the interpretation of the scattering mechanism.

To reduce speckle effects and improve classification results, the Lee filter was applied on the above images several times, each time increasing the size of the moving window. The ML classification was performed on the despeckled images. Classification accuracy pointed out the most appropriate size of the filter window for speckle reduction.

1. INTRODUCTION

Full polarimetric data can define the scattering behaviour of land use/cover, thus giving better land use/cover classification results than single-channel SAR (Smith, Broek, Dekker, 1998). Several parameters have been proposed to assist the interpretation and the classification of polarimetric SAR data. These parameters are deduced from the decomposition of either the complex voltage reflection matrix or the power reflection matrices. The first decomposition category deals with the sphere/deplane/helix decomposition and the Pauli decomposition. The latter category can be divided into the Muller/Kennaugh matrix and covariance or coherency matrix (Hellmann, 1999). Among them the basic Cloude-Pottier parameters, entropy and alpha, (Cloude, Pottier, 1997) deduced from the Cloude decomposition theorem applied on the coherency matrix are the most investigated (Hellmann, Kratzschmar, 1998; Titin-Schnaider, 1999; Scheuchl, Caves, Cumming, Staples, 2001) for land use/cover interpretation. The number of these parameters was farther increased by the addition of two polarizing parameters, the propagation and helicity phase angles and three depolarising parameters, the anisotropy A and two depolarising eigenvector angles (Cloude, Potier, Boerner, 2002). Parameters deduced by the span normalisation of the Mueller matrix have also been investigated in order to retrieve scattering electromagnetic mechanisms (Titin-Schnaider, 1999) and interpret polarimetric data.

Based on the coherency matrix, the complex Wishart classifier, which uses the complex Wishart distribution of the coherency

matrix and measures an appropriate distance, d , according to maximum likelihood classification (Lee, Grunes, Kwok, 1994), has been investigated for supervised land use/cover classification (Lee, Liew, Kwok, Nakayama, 2001). An unsupervised classification method based on the Wishart classifier was also developed (Scheuchl, Caves, Cumming, Staples, 2001), as well as, a weighed Wishart classifier according to which each polarimetric component is weighed relative to the absolute amplitude of the measurements (Smith, Broek, Dekker, 1998).

Focusing on the evaluation of the polarimetric information deduced by the simplest processing methods, the objectives of this work are to:

1. Interpret land use/cover scattering behaviour by analysing the a) polarization signatures regarding to the ellipticity angle, orientation and intensity, and b) signatures extracted by the Pauli decomposition method
2. Classify land use/cover of the test area based on the magnitude content of a) the original full polarimetric data, b) the data produced by the Pauli decomposition method, and c) both previous cases data.
3. Define the most appropriate size of the Lee filter window, applied for speckle reduction.

The full polarimetric airborne data sets were acquired with DLR's Experimental SAR (E-SAR). The test region is the area of Oberpfaffenhofen, Germany. For the study needs, the L band was used which has a resolution of 3 meters.

2. POLARIZATION AND PAULI DECOMPOSITION THEORY

2.1 Wave Polarization

For a plane transverse electromagnetic wave, the \vec{E} vector of the electric field oscillates in a plane perpendicular to the propagation direction. The vectorial nature of these waves is called polarization and is independent of the chosen coordinate system. In the case that the trace of the tip of the field vector \vec{E} within a plane perpendicular to the propagation direction is an ellipse, the wave is elliptically polarized. Special cases of the elliptically polarization are linear or circular polarization. For the description of polarization, a coordinate system and a reference direction of propagation are needed. For compatibility with fully polarimetric radar systems that use two orthogonal linear polarized antennas, a Cartesian coordinate system is introduced, where $+\vec{k}$ is the propagation direction of the plane transverse electromagnetic wave, and \vec{h} and \vec{v} are the horizontal and vertical directions of the plane of the electric field. The equation of a transverse electromagnetic wave as a function of its position \vec{r} is:

$$\vec{E}(\vec{r}) = \vec{E} \exp(i\vec{k} \cdot \vec{r}) \quad (1)$$

The vector \vec{E} of the complex electric field consists of a $\vec{h}E_h$ component and a $\vec{v}E_v$ component, which are perpendicular to the propagation direction.

$$\vec{E} = \vec{h}E_h + \vec{v}E_v \quad (2)$$

These components can be expressed on the basis of their real amplitude $a_j = |E_j|$ and phase $\exp(i\delta_j)$:

$$\vec{E}_j = \vec{j} \cdot \vec{E} = a_j \exp(i\delta_j) \quad (3)$$

where $j = h$ or v . The component E_j of the electric field can also be written as a function of time t and position r :

$$E_j(\vec{r}, t) = \text{Re}\{E_j \exp(i\vec{k} \cdot \vec{r} - \omega t)\} = \text{Re}\{a_j \exp(i\vec{k} \cdot \vec{r} - \omega t + \delta_j)\} = a_j \cos(\vec{k} \cdot \vec{r} - \omega t + \delta_j) = a_j \cos(\tau + \delta_j) \quad (4)$$

where $\tau = \vec{k} \cdot \vec{r} - \omega t$. By defining angle δ as the relative phase difference between the two components, $\delta = \delta_v - \delta_h$, it results that:

$$\begin{aligned} \frac{E_v(\vec{r}, t)}{a_v} &= \cos(\tau + \delta + \delta_h) = \cos(\tau + \delta_h) \cos \delta - \sin(\tau + \delta_h) \sin \delta \\ &= \cos(\tau + \delta_h) \cos \delta - \sqrt{1 - \cos^2(\tau + \delta_h)} \sin \delta \end{aligned} \quad (5)$$

Substituting $\cos(\tau + \delta_h)$ by equation (4) we obtain:

$$\frac{E_v(\vec{r}, t)}{a_v} = \frac{E_h(\vec{r}, t)}{a_h} \cos \delta - \sqrt{1 - \frac{E_h^2(\vec{r}, t)}{a_h^2}} \sin \delta$$

$$\Rightarrow \frac{E_v(\vec{r}, t)^2}{a_v^2} + \frac{E_h(\vec{r}, t)^2}{a_h^2} - 2 \cos \delta \frac{E_v(\vec{r}, t)E_h(\vec{r}, t)}{a_v a_h} = \sin^2 \delta \quad (6)$$

which is the equation of an ellipse (figure 1) with an orientation angle ψ such that

$$\tan(2\psi) = \frac{2a_v a_h}{a_v^2 - a_h^2} \cos \delta \quad (7)$$

Consequently, polarization may also be described by the geometrical properties of the ellipse which are the orientation angle ψ and the ellipticity angle χ

$$\tan(\chi) = \pm \frac{a}{b} \quad (8)$$

where $2a$ and $2b$ are the minor and major axes of the ellipse, and χ specifies the shape of the ellipse as well as the sense of rotation of the vector \vec{E} . The polarization is left handed for $0 < \chi < \pi/4$ and right handed for $-\pi/4 < \chi < 0$ for an observer looking in the direction of the propagation. The polarization angles ψ and χ are related to the wave parameters a_v , a_h , and δ by

$$\begin{aligned} \sin(2\chi) &= \sin(2\alpha) \sin(\delta) \\ \tan(2\psi) &= \tan(2\alpha) \cos(\delta) \end{aligned} \quad (9)$$

where the angle α is defined as

$$\tan(\alpha) = \frac{a_v}{a_h} \quad (10)$$

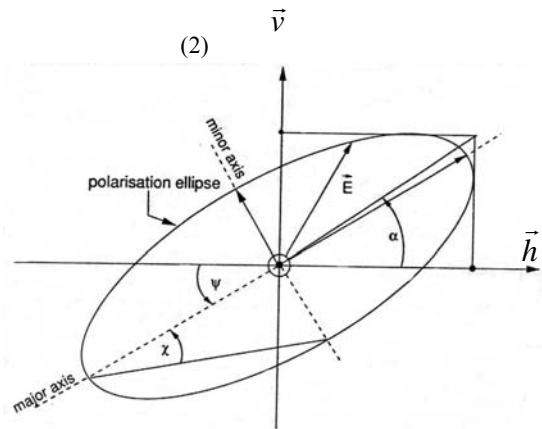


Figure 1. Wave elliptically polarized in (\vec{h}, \vec{v}) plane with propagation direction $+\vec{k}$

If both amplitudes are equal $a_v = a_h$, and $\chi = \pm \pi/4$, the polarization is circular. For $\chi = +\pi/4$ the polarization is left hand circular and for $\chi = -\pi/4$ the polarization is right hand circular.

In the case that the phase angles are equal $\delta_v = \delta_h \rightarrow \delta = 0$ the trace of the tip of the electric field vector \vec{E} is a straight line.

2.2 The Pauli decomposition approach

If a scatterer is illuminated by an electromagnetic plane transmitted by an antenna, the incident wave at the scatterer is given by

$$\vec{E}^{ir} = \vec{h} E_h^{ir} + \vec{v} E_v^{ir} \quad (11)$$

and that induces currents in the scatterer, which in turn reradiate a scattered wave. In the far zone of the scatterer, the scattered wave can be considered as a plane wave. The scattering process can be modelled as a linear transformation, described by a matrix S. The received field is then given by:

$$\vec{E}^{re} = [S] \vec{E}^{ir} = \begin{bmatrix} E_h^{re} \\ E_v^{re} \end{bmatrix} = \frac{\exp ikr}{r} \begin{bmatrix} S_{hh} & S_{hv} \\ S_{vh} & S_{vv} \end{bmatrix} \begin{bmatrix} E_h^{ir} \\ E_v^{ir} \end{bmatrix} \quad (12)$$

The [S] matrix is referred to as Jones matrix (Jones, 1941), and is a complex 2x2 matrix, containing information on the scatterer. S_{hh} and S_{vv} are called co-polar and S_{hv} and S_{vh} cross-polar components. According to the reciprocity theorem, the cross-polar components are equal.

Instead of the matrix notation, one may use a four element complex vector \vec{k} , which contains complete information on the [S] matrix.

$$[S] = \begin{bmatrix} S_{hh} & S_{hv} \\ S_{vh} & S_{vv} \end{bmatrix} \rightarrow \vec{k} = \frac{1}{2} \text{Trace}([S]\Psi) = [k_0, k_1, k_2, k_3]^T \quad (13)$$

where Trace ([S]) is the sum of the diagonal elements of [S] and Ψ is a complete set of 2x2 complex basis matrices under a hermitian inner product. Any complete orthonormal basis set of four 2x2 matrices can be used. A basis which is more related to the physics of wave scattering, the Pauli basis, is formed by the Pauli spin matrices (Cloude, 1986).

$$\Psi_p = \left\{ \sqrt{2} \begin{bmatrix} 1 & 0 \\ 0 & 1 \end{bmatrix}, \sqrt{2} \begin{bmatrix} 1 & 0 \\ 0 & -1 \end{bmatrix}, \sqrt{2} \begin{bmatrix} 0 & 1 \\ 1 & 0 \end{bmatrix}, \sqrt{2} \begin{bmatrix} 0 & -i \\ i & 0 \end{bmatrix} \right\} \quad (14)$$

The corresponding vector \vec{k}_p is then

$$\vec{k}_p = \frac{1}{\sqrt{2}} [S_{hh} + S_{vv}, S_{hh} - S_{vv}, S_{hv} + S_{vh}, i(S_{vh} - S_{hv})]^T \quad (15)$$

The Pauli decomposition approach assigns the appropriate deterministic scattering mechanisms to each one of the four elementary scattering matrices. The basic scattering mechanisms are: isotropic surface, right wound helix and left wound helix. Consequently, the Pauli matrices can be interpreted as shown in table 2 (Hellmann, 1999).

Pauli matrix	Scattering type	Interpretation
$\begin{bmatrix} 1 & 0 \\ 0 & 1 \end{bmatrix}$	odd-bounce	Surface, sphere, corner reflectors
$\begin{bmatrix} 1 & 0 \\ 0 & -1 \end{bmatrix}$	even-bounce	dihedral
$\begin{bmatrix} 0 & 1 \\ 1 & 0 \end{bmatrix}$	even-bounce titled 45°	45° titled dihedral
$\begin{bmatrix} 0 & -i \\ i & 0 \end{bmatrix}$	cross-polariser	Not existent for backscattering

Table 2. Pauli matrices and their interpretation in the (\vec{e}_h, \vec{e}_v) polarization basis

3. INTERPRETATION OF THE POLARIMETRIC DATA

3.1 Interpretation of polarization signatures

A polarization signature is given by its 3-D presentation. X, Ψ , Z axes are assigned to the ellipticity angle χ , the orientation angle ψ , and the intensity of the co-polar or cross-polar components of the radar signal (Z). As mentioned previously, the ellipticity angle takes values in the interval $[-45^\circ, 45^\circ]$ and the orientation angle in the interval $[0, 180^\circ]$. Polarization signatures were extracted for four land uses: urban, forest, vegetation, and smooth surfaces (roads, runways, etc).

The signature of the urban class presents high values of intensity for an ellipticity angle close to 45° and an orientation angle close to 180° (figure 3). This means that polarization is left hand circular (i.e. the amplitudes of the co-polar components S_{hh} and S_{vv} are equal and the relative difference angle close to 90°), and the orientation of the wave transmitted changes 180° relative to the orientation of the wave received. The above description fits well to the even-bounce scattering type of horizontal dihedrals, which correspond to the building-ground interaction that we encounter in urban areas.

In figure 3 we also observe very low values of intensity for an ellipticity angle close to 0° and an orientation angle close to 0°. This means that in urban areas, polarization horizontally oriented, which is the dipole like scattering case, is missed. The low intensity values for an ellipticity angle close to -45° and an orientation angle close to 0° denote the surface scattering type of smooth surfaces (e.g. roads) found in the urban areas.

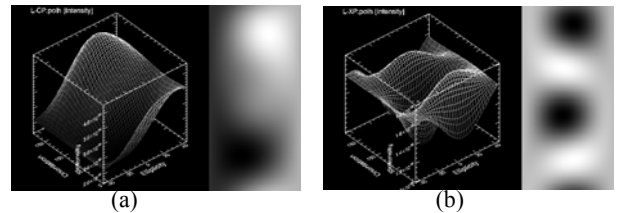


Figure 3. a) The co-polar and b) the cross-polar signature of the urban area

Urban areas also have large cross-polar contribution (figure 3). The range entire of values of the ellipticity angle is encountered for high intensity of the cross-polar components and for an orientation angle close to a) 29°, and b) 162°. This proves that discontinuities of both scattering types, dihedrals and surfaces, result in random polarization ellipses. Those with an orientation

compatible with the radar look angle present the highest values in the cross-polar signature. The case of $\pi/4$ titled dihedrals is little presented in this figure, for high intensity of the cross-polar components, an ellipticity angle equal to 45° and an orientation angle close to 180° .

In the forest co-polar signature, the highest values of intensity are observed for an ellipticity angle close to 0° , and an orientation angle close to 160° (figure 4). In this case, polarization is almost horizontally oriented (i.e., S_{hh} presents high value and S_{vv} a value close to 0). Consequently, several areas in the forest environment denote a dipole like scattering, resulting from the a) volume scattering, i.e. wave scattered by branches and/or leaves, b) contribution of two scattering types, dihedral and surfaces. The latter occurs because a resolution cell can represent either a trunk to ground interaction which denotes the double scattering mechanism, or a uniform smooth area which denotes a surface scattering mechanism. Although forest leaves are randomly oriented, they fit more to horizontal dipoles. Thus, the forest signature presents low values of co-polar intensity for an ellipticity angle close to 0° and an orientation angle close to 70° (figure 4), i.e. for waves that are vertically polarized (S_{vv} presents a high value and S_{hh} a value close to 0). In the forest cross-polar signature (figure 4), like in that of urban areas, the radar look angle defines the orientation of high cross-polar intensities. The case of $\pi/4$ titled dihedrals is strongly presented in this figure for high intensity of the cross-polar components, an ellipticity angle equal to 45° and an orientation angle close to 180° .

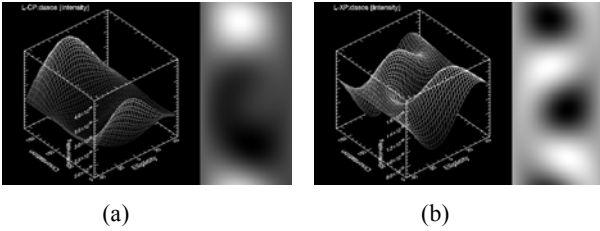


Figure 4. a) The co-polar and b) the cross-polar signature of the forest area

In the vegetation co-polar signature, we observe high values of intensity for an ellipticity angle close to 0° , and orientation angles close to 160° and 80° respectively (figure 5). This means high return of the wave scattered by horizontally and/or vertically oriented dipoles. The low intensity values, which we observe for an ellipticity angle close to -45° and an orientation angle close to 0° , denotes the surface scattering type of smooth surfaces like bare soil or sowed fields. In contrast to the forest signature, vegetation signature denotes an organization of the

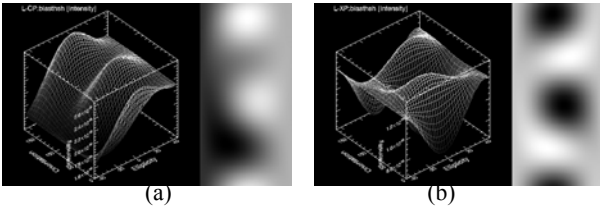


Figure 5. a) The co-polar and b) the cross-polar signature of the vegetation

scatterers which allows them to act either as horizontal (leaves) or vertical (trunks) dipoles. In the vegetation cross-polar signature (figure 5), the case of $\pi/4$ titled dihedrals is strongly presented.

In the runway co-polar signature (figure 6), the lack of returned wave is observed for almost the entire range of values of the ellipticity angle, i.e. for random ellipses. Indeed, low intensity values are observed for an orientation angle close to 0° .

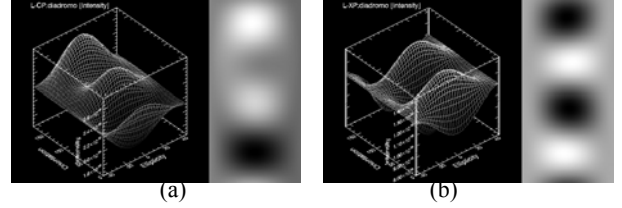


Figure 6. a) The co-polar and b) the cross-polar signature of the runway

Furthermore, this signature is similar to that of the vegetation - dipole like scattering - presenting, however, lesser intensity values. Dipoles are formed along the runway by the contribution of two scattering types, dihedral and surfaces. This occurs because a resolution cell can represent either a grass to ground interaction which denotes the double scattering mechanism, or a uniform smooth area which denotes the runway surface. In the runway cross-polar signature (figure 6), the case of $\pi/4$ titled dihedrals is slightly presented.

3.2 Interpretation of the Pauli signatures

The Pauli components are computed as following:

$$\begin{aligned} \text{Pauli 1} &= S_{hh} - S_{vv} \\ \text{Pauli 2} &= S_{hv} + S_{vh} \\ \text{Pauli 3} &= S_{hh} + S_{vv} \end{aligned} \quad (16)$$

where Pauli1 denotes the even bounce component, Pauli2 the 45° titled even bounce component, and Pauli3 the odd bounce component. For each of the 3 components we calculate the absolute value, we scale it with an exponent of 0.7 and assign a color. Red color is assigned to Pauli1, green to Pauli2, and blue to Pauli 3. Pauli signatures are extracted from the color composition of the three components.

For the urban area the red color, i.e. dihedrals, dominates (figure 7). The orientation of the streets is consequently extracted. Surface scattering type (green) and 45° titled dihedrals (blue) are less presented. There are also areas in which all the scattering mechanisms detected by the Pauli method are simultaneously presented. These areas are shown with white

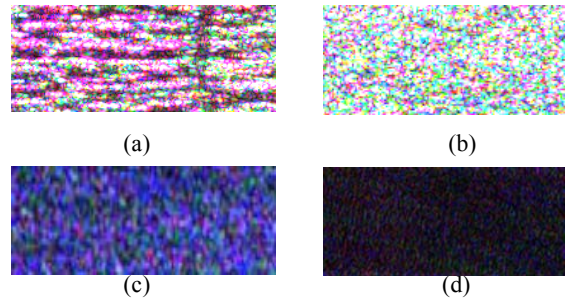


Figure 7. Color composition of the Pauli analysis for the a) urban, b) forest, c) vegetation, and d) runway class

color. In the forest signature, colors are equally presented, i.e. none of the scattering mechanisms which are detected by the Pauli method, dominates. In the vegetation signature, the blue colour dominates. This means that the surface scattering type is the most presented. The runway signature is presented by dark tones. This means that none of the scattering type dominates.

4. CLASSIFICATION

4.1 Classification based on original polarimetric data

Based on the absolute value of the S_{hh} and S_{vv} and $(S_{hv} + S_{vh})/2$ of the polarimetric components, we applied the supervised Maximum Likelihood classifier in order to classify the study area into four classes: urban, forest, vegetation, and runways. Classification was applied a) on raw data and b) on data without speckle, generated by the application of the Lee filter. In order to investigate the most appropriate window size, we first applied the Lee filter 9 times, each time increasing the size of the window by a step equal to 2. The windows used were 3x3, 5x5, ... 17x17. Then classifications were performed, and their accuracy was calculated based on a set of test areas. The total accuracy of the classification applied on the raw data is 83.60%, and the results obtained after the Lee filter application are given in figure 8.

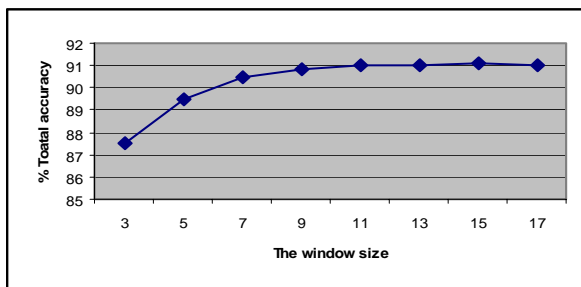


Figure 9. % Total accuracy of the polarimetric data based classification as a function of the size of the Lee filter

We observe that the highest accuracy, 91%, is obtained for a window size 15x15. In this classification, the accuracy obtained for the class of the: urban area is 45,84%, forest 94.72%, vegetation 95.43%, and runway 99.32%. The urban class is most confused with the forest. Although the polarization signatures of the two categories are quite different (figure 3 and 4), due to the fact that Bayes classifier is based on the magnitudes only, the urban and forest classes are confused. For the other classes, the magnitude based classification produces high accuracies.

4.2 Classification based on Pauli decomposition analysis

Bayes classifier was also applied on the absolute values of the three Pauli decomposition components, by using the same training set as in the previous classification. Classification was applied a) on the initial Pauli components, and b) on the Pauli components after the application of the Lee filter. The most appropriate window size was investigated by the method described in the previous section. Accuracy was tested by the same test set as in the previous classification. The total accuracy of the classification applied on the initial Pauli components is 80.00%, and the results obtained after the Lee filter application are given in figure 9.

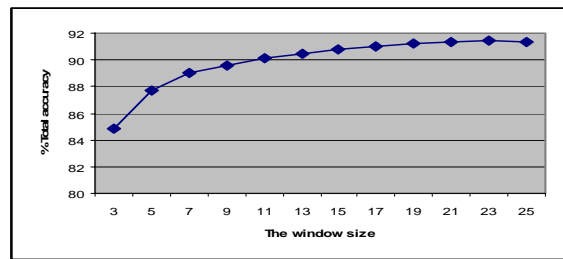


Figure 9. % Total accuracy of the Pauli based classification as a function of the size of the Lee filter

We observe that the highest accuracy, 91.41%, is obtained for a window size 23x23. In this classification, the accuracy obtained for the class of the: urban area is 81,08%, forest 78.06%, vegetation 97.35%, and runway 99.01%. The urban and forest classes are confused. Although the accuracy for the urban class is significantly increased in comparison to the classification based on original polarimetric data, the accuracy of the forest class is reduced. The scattering mechanisms that Pauli decomposition analyzes, and especially the even bounce and 45° titled even bounce mechanisms, reinforce the discrimination of the urban class. On the other hand, the weakness of the Pauli decomposition in analyzing the volume scattering mechanism (based on dipoles) affects the accuracy for the forest class, which is analyzed on the basis of dihedrals. For the other classes, the Pauli based classification produces high accuracies.

4.3 Classification based on original and Pauli decomposition analysis

To reduce confusion between urban and forest areas, Bayes classifier was applied on the absolute values of the a) polarimetric data, and b) data generated by Pauli decomposition analysis. In this way, odd and even bounce scattering mechanisms, as well as, original full polarimetric information participate in a magnitude based classification. Classification was applied a) on the initial data, and b) on data after the application of the Lee filter. The most appropriate window size was investigated by the method described in section 4.1. Accuracy was tested by the same test set as in the previous classification. The total accuracy of the classification applied on the initial data is 82.14%, and the results obtained after the Lee filter application are given in figure 10.

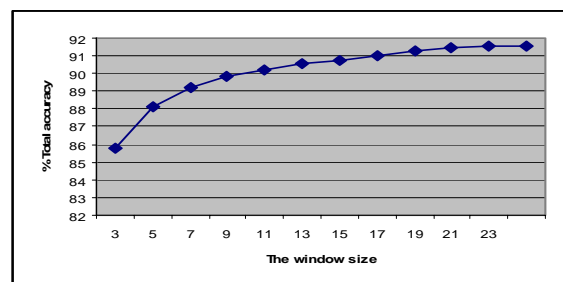


Figure 10. % Total accuracy of the classification as a function of the size of the Lee filter

We observe that the highest accuracy, 91.53%, is obtained for a window size 23x23. In this classification the accuracy obtained for the class of the: urban area is 81,65%, forest 78.31%, vegetation 97.20%, and runway 99.25%. The accuracy of the urban class is slightly increased although urban and forest class

are still confused. Urban pixels classified as forest account for 18.19% of the urban sample. Forest pixels classified as urban account for 21.69% of the forest sample.

5. CONCLUSIONS

The potential of the polarimetric data to discriminate among different land uses was investigated in this study. Simple processing methods, such as extraction of polarimetric signatures and Pauli decomposition analysis were used to interpret the scattering mechanisms of each land use. Polarimetric signatures were proved to be a powerful tool for this purpose. Several scattering mechanisms have been recognized on each signature. The large number of scattering mechanisms produced by non-deterministic targets, such as samples of land use, was their main disadvantage. Although given a polarimetric signature we can recognize the scattering behaviour of the specific land use, the opposite is sometimes difficult to achieve. Due to the large number of scattering centres that a land use sample includes, several secondary scattering mechanisms are simultaneously produced. This can make it difficult for the interpreter to distinguish the most characteristic mechanism for the sample under interpretation.

The non deterministic nature of land use targets was also indicated by the Pauli decomposition analysis. Dihedrals and surface are the scatterers that Pauli decomposition can determine. The limited number of scattering mechanisms recognized by the Pauli analysis is its main disadvantage. Its ability to indicate dihedrals is its main advantage. Urban areas which present a complexity by including several different scattering centres in the same target can easily be interpreted after their analysis in dihedrals.

Regarding the definition of the size of the window of the Lee filter which is used for speckle suppression, a classification based method was developed and applied. Due to the non deterministic approach of the scatterers, the optimum size of the window has been found to be quite large, 17x17 pixels for the original data and 23x23 pixels for the data sets which include images generated by the Pauli decomposition method. This documents the non deterministic nature of land uses, as a large filter window is necessary for high classification accuracies to be achieved.

To evaluate classifications based on the magnitude of the polarimetric data, the maximum Likelihood classifier was applied on a) the full polarimetric data, b) the data produced by the Pauli decomposition method, and c) both previous cases data. In all cases speckle suppression preceded. The total accuracies obtained in all cases were satisfactory (91-91.53%). The very high resolution of the E-SAR data also contributed to this. However, the accuracy obtained for the urban class was mediocre (45.84%) in the first classification results, pronouncing the weakness of the magnitude of the polarimetric data to discriminate urban areas from forest. The data generated by Pauli decomposition contributed to the improvement of classification results regarding the urban class, producing an accuracy equal to 81.08% and 81.65% for classifications b and c, respectively. On the other hand, they reduced the accuracy of the forest class by approximately 15%, (78.31%). Dihedrals are well discriminated by the Pauli analysis and characterize the urban class more than other classes. When the images generated by the Pauli decomposition are introduced in the Maximum Likelihood classification contribute significantly to the

statistical definition of this category but they produce misclassifications to the other categories which also contain dihedrals, such as the forest.

The key subject for further work will be the introduction of the phase of the full polarimetric data in the classification algorithm.

REFERENCES

- Cloude, S.R., Pottier, E., Boerner W., 1997. Unsupervised Image Classification using the Entropy/Alpha/Anisotropy Method in Radar Polarimetry. In *AIRSAR Earth Science and applications Workshop*, March 1997.
- Cloude, S.R., Pottier, E., 1997. An entropy based classification scheme for land applications of polarimetric SAR. *IEEE Transactions on Geoscience and Remote Sensing*, Vol 35, n°1, pp. 68-78.
- Hellmann, M., 1999. Classification of Full Polarimetric SAR-Data for Cartographic Application. Thesis, Technical University of Dresden, August 1999.
- Hellmann, M., Kratzschmar, E., 1998. Interpretation of SAR-Data using Polarimetric Techniques. In: *The retrieval of Bio- and Geo-physical parameters from SAR Data for land application Workshop*, ESTEC, 21-23 October 1998.
- Lee, K.Y., Liew, S.C., Kwoh, L.K., and Nakayama, M., 2001. Land Cover Classification Using NASA/JPL Polarimetric Synthetic Aperture Radar (POLoSAR) Data. In *the 22nd Asian Conference on Remote Sensing*, Singapore, 5-9 November 2001.
- Lee, J.S., Grunes, M., Kwok, R., 1994. Classification of multi-look polarimetric SAR imagery based on complex Wishart distribution. *International Journal of Remote Sensing*, Vol. 15, no 11, pp. 2299-2311.
- Scheuchl, B., Caves, R., Cumming, I., and Staples, G., 2001. Automated Ice Classification Using Spaceborne Polarimetric SAR Data. In: *IGARSS Proceedings*, Australia.
- Smith, A. J., van den Broek, A. C., and Dekker R. J., 1998. Landuse Classification Using PHARUS Polarimetric Radar. In *Proceedings of the 2nd International Workshop on Retrieval of Bio- & Geo-physical Parameters from SAR Data for Land Applications*, 21-23 October 1998, Netherlands.
- Titin-Schnaider, C., 1999. Radar polarimetry for vegetation observation. In: *CEOS SAR Workshop*, Netherlands, 26-29 October 1999.

ACKNOWLEDGEMENTS

Authors are grateful to Dr J. Moreira (DLR) who kindly provided the E-SAR polarimetric data.